RANS COMPUTATIONS OF FLOW AROUND A BULK CARRIER WITH ENERGY SAVING DEVICE

Artur Lidtke (University of Southampton, UK)
Arun P. Lakshmynarayanana (University of Southampton, UK)
Josef Camilleri (University of Southampton, UK)
Charles E. Badoe (University of Southampton, UK)
Joseph Banks (University of Southampton, UK)
Alexander B. Phillips (National Oceanographic Centre, UK)
Stephen R. Turnock (University of Southampton, UK)

1. SUMMARY

The Fluid Structure Interactions group (University of Southampton) has been extensively involved in many research projects focusing on computations of ship wake field and the interactions between the propeller, rudder and the hull. A finite-volume RANS code, OpenFOAM (OpenFOAM, 2014) has been used mostly in majority of these works. The goal of the group has been to improve the in-house capability of prediction of ship stern flows using open-source software. In the present work OpenFOAM is benchmarked against a commercial code, Star-CCM+ (Star-CCM+, 2012), with the aim of exploring the differences in flow field results originating from particular features of both implementations.

The Japan Bulk Carrier (JBC) has been chosen as a test case representative of the challenges faced in modern ship flow modelling. This vessel is fitted with an energy saving duct. The JBC case is part of the Tokyo 2015 CFD workshop and the latest in the series of benchmarking workshops to assess the state of art of marine CFD (Larsson et al., 2014). All computations are performed under steady state, fixed (even keel) conditions using identical grids and similar numerical setup. Presented analysis focuses on the mean flow, vortical structures and global hull forces.

2. INTRODUCTION

This work investigates and compares results obtained using the commercial Reynolds Averaged Navier Stokes (RANS) flow solver Star-CCM+ and its open source counterpart OpenFOAM in the context of stern flow computation of the model scaled JBC hull form with energy saving device (duct). The main focus of the paper is to perform a detailed comparison of both codes in the prediction of the mean flow field and global forces. In order to carry out a like for like comparison, effort has been placed on using similar parameters, such as grid and numerical settings, for both codes. The only notable difference observed results from the treatment of the wall. All y+ wall treatment has been used in the computations with Star-CCM+ whilst the OpenFOAM code fully resolved the boundary layer.

3. GEOMETRY, CONDITIONS AND EXPERIMENTAL DATA

The JBC (Japan Bulk Carrier) ship geometry (see Fig 1 and Table 1) equipped with a stern duct as an energy saving device (ESD) is considered at model scale (1:40). Full details of the geometrical parameters are available at the Tokyo 2015 website (www.t2015.nmri.go.jp). The ship is also equipped with a propeller, but not a rudder. In the present calculations Test cases 1.3, 1.4 and 1.6 of the Tokyo workshop were considered, namely towed condition in calm water, without/with ESD and self-propulsion in calm water conditions without ESD, respectively. All conditions studied correspond to Froude number Fn=0.142 and the propeller rps is fixed at the experimentally obtained value of 7.8 in the self-propelled simulations. Forces, moments and mean flow data were provided by the National Maritime Research Institute (NMRI, 15).

4. THEORETICAL APPROACH

4.1 RANS Formulation

The flow generated around the hull and duct is modelled using the Reynolds Averaged Navier-Stokes equations. Within the assumption of an incompressible fluid, the set of equations may be written in the form:-

$$\frac{\partial \overline{U_i}}{\partial x_i} = 0, \qquad [1]$$

$$\frac{\partial \overline{U_i}}{\partial t} + \frac{\partial \overline{U_i}\,\overline{U_j}}{\partial x_j} = -\frac{1}{\rho}\frac{\partial \overline{P}}{\partial x_i} + \frac{\partial}{\partial x_j}\left\{\nu\left(\frac{\partial \overline{U_i}}{\partial x_j} + \frac{\partial \overline{U_j}}{\partial x_i}\right)\right\} - \frac{\partial \overline{u'_i u'_j}}{\partial x_j} + \overline{f_i} \qquad [2]$$

where x_i represents the Cartesian coordinates (X, Y, Z) and $\overline{U_i}$ are the Cartesian mean velocity components ($\overline{U_x}$, $\overline{U_y}$, $\overline{U_z}$). The Reynolds stress is expressed as ($\overline{u'_i u'_j}$) and must be modeled using an appropriate turbulence model. The SST k-ω model has previously been successfully used for this purpose of hull-propeller-rudder interaction and wakefield analysis, (Larsson et al., 2014) making it a natural choice for the study discussed herein.

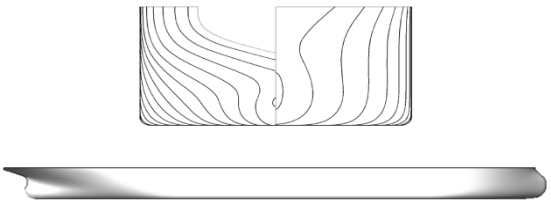

Fig.1 Sections (top) and profile view (bottom) of bare hull of JBC (NMRI, 15).

Table 1 Principal parameters of the JBC

Parameters	JBC without ESD	JBC with ESD
L_{pp}(m)	7	7
B_{WL}(m)	1.125	1.125
T(m)	0.4	0.4
F_n	0.142	0.142
$S_O / {L_{PP}}^2$	0.249	0.250
Propeller parameters		
D(m)	0.203	0.203
n(rps)	7.8	7.5

The RANS equations were solved with both codes on a body-fitted multi block structured grid by means of cell centered finite volume method (FVM). Discretisation of the convection terms were achieved using Gauss linear second order upwind and the diffusion terms were treated using the central difference scheme. The SIMPLE algorithm was used for solving the pressure-velocity coupling. First-order schemes were applied to the turbulent quantities. Table 2 presents the computational settings adopted for both Star-CCM+ and OpenFOAM.

4.2 Propeller model

In order to reduce the cost in self-propelled computations, a body force propeller was used for both codes instead f it being fully resolved.

In the OpenFoam computation, the impact of the propeller on the fluid is represented as a series of axial and tangential momentum sources. Their strength is then calculated using the Hough and Ordway thrust and torque distribution, (Hough and Ordway, 1965). This closely matches the optimum distribution, Goldstein, (1929).

Initially no momentum sources were applied, by setting the propeller revolutions (rps) to zero. The resulting nominal wake fraction is determined once a converged solution is achieved by sampling the velocities entering the propeller plane. The momentum sources were then calculated based on the propeller rps and the openwater characteristics. The simulations are then started from the naked hull solutions but now with the added momentum sources (both axial and tangential momentum terms) and run until convergence is achieved.

In the Star-CCM+ computations, a virtual disc propeller model with principle and load distribution similar to that outlined in OpenFOAM was used to account for the action of the rotating propeller.

Table 2 Computational parameters

Parameters	Settings	
	OpenFOAM	Star-CCM+
Mesh Type	Structured	Structured
No of Elements	19.44M (w/o ESD)	19.44M (w/o ESD)
	21.26M (with ESD)	21.26M (with ESD)
y^+ average	<1	<1
Turbulence model	Shear Stress Transport, Menter, (1994)	Shear Stress Transport, Menter, (1994)
Wall modelling	Wall resolved	Low y+ (wall resolved)
Convergence criteria	RMS residual $< 10^{-7}$	RMS residual $< 10^{-7}$
Computing	Iridis 4 Linux cluster	Iridis 4 Linux cluster
Run type	Parallel (16 partitions run on 4x Dual core nodes)	Parallel (16 partitions run on 4x Dual core nodes)

5. COMPUTATIONAL GRID

Structured, hexahedral meshes created using Pointwise were used for both Star-CCM+ and OpenFOAM. To enable faster computations, cases without self-propulsion were ran using a symmetry boundary condition at the center plane of the vessel, halving the mesh count. All grids were designed with y+<1 over the entire surface of the ship, thus allowing the boundary layer to be computed without the use of wall functions. Due to the low Froude number (Fn=0.142) a symmetry plane condition was used on the free surface, thus allowing a single-phase simulation to be used.

Particular challenge in the mesh design was to accommodate the energy saving device without causing strong non-orthogonality of the cells whilst meeting the wall-normal cell size requirements. An outline of the final configuration, showing the definition of individual mesh blocks, is shown in Fig. 2. Resolving the vortical structures onset to the propeller plane also required sufficient mesh density in the outer boundary layer regions near the stern, as shown in Fig. 3 for measurement station 4 with (left) and without (right) the ESD, respectively. Total cell counts used in the considered grids is shown in Table 3.

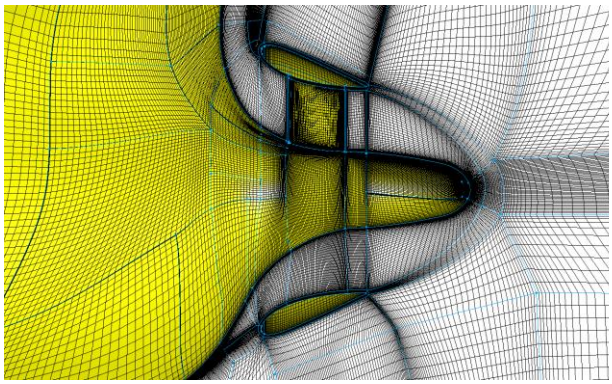

Fig.2 Structure of the final mesh around the JBC hull with duct, showing local refinement regions near hull, near duct and in the wake regions.

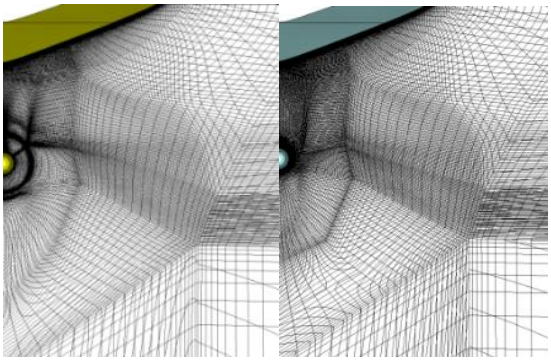

Fig.3 Structure of the final mesh around the propeller plane and wake region with (left) and without (right) the ESD.

Table 3 Grids used for computations(cell counts quoted for half body)

Grid	Size
Coarse without ESD	4.03M
Fine without ESD	9.72M
Fine with ESD	10.63M

6. RESULTS

6.1 Resistance

Table 4 compares the total towed resistance with and without ESD between Star-CCM+ and OpenFOAM. Both codes predicts the towed drag within reasonable error margins. An important observation is that OpenFOAM correctly capture the reduction of drag caused by the ESD but Star-CCM+ simulation showed an inverse trend.

Due to the low operating Froude number of the JBC (Fn= 0.142), wave resistance was neglected in all computations. However a quick estimate of the wave resistance using existing non-linear potential flow code (Courser et al., 1998) resulted in R_W of 4.1033N without the ESD. As the wave drag estimate has not been compared with the experiment this must be treated with caution.

Table 4 Summary of ship resistance prediction with and without ESD (final grid)

Parameter	EFD	OpenFOAM	StarCCM+
Without ESD			
$C_T \times 10^3$	4.289	4.318	4.196
$C_F \times 10^3$		3.328	3.244
$C_P \times 10^3$		0.990	0.952
With ESD			
$C_T \times 10^3$	4.263	4.259	4.246
$C_F \times 10^3$		3.314	3.273
$C_P \times 10^3$		0.946	0.970

6.2 Flow pattern

Limiting streamlines on the hull surface are shown in Figures 4 and 5 for the OpenFOAM simulations. A complex flow pattern can be seen both with and without the ESD, with regions of reversed flow and converging streamlines. Without the duct present (Fig 4a), the flow coming from underneath the ship may be seen to separate around the area of high curvature (shown as area B). Higher above the keel the flow may be seen to approach the separation zone from the top. A secondary separation zone may be seen between points A and C and further downstream along the shaft line and the hub. This is most likely associated with the flow from the upper parts of the hull encountering high curvature. Flow divergence can also be seen at the saddle point (marked as D). Addition of the duct (Fig 5a) may be seen to significantly reduce the size of the separation zone associated with separation from the bilge by virtue of inducing a more favourable pressure gradient. More regular flow may also be seen below the propeller hub. Notice how the addition of the propeller (see Figs 4b &5b) affect the flow behavior described above.

Vortical structures for the case without duct in Fig 6a-c show a strong vortex at the propeller plane due to separation from the bilge downstream of the aft shoulder, confirming the observations drawn from analysing the limiting streamlines. The extent of the separation zone below the propeller hub may also be more clearly visualised, indicating that it may cause a substantial amount of non-uniformity of propeller inflow. It is interesting to note how the duct (Figs 7a-c) interacts with this separated flow region, equalising the flow.

6.3 Axial velocity predictions

The axial velocity field prediction at the stern for the towed condition with duct using the both codes is shown in Figs 8 and 9. In general, there was very little difference between the flow field generated by both codes (an example provided by Fig8). A less intense bilge vortex is predicted using the SST k-ω model compared with the experiments.

Star-CCM+ (Fig 9) showed much improved wake behind the duct.

7. SELF-PROPULSION

The self-propelled test was conducted without the ESD for both codes by keeping the rate of rotation of the propeller fixed. The results are presented in Figs 10&11. Both codes produced similar results. The influence of the propeller on the axial velocity upstream of the propeller disk in Fig 10 shows reasonable agreement with experiment. This may be due to the fact that the location may be too far to locate any localized upstream effect of the propeller.

Close to the propeller plane in Fig 11, the difference due to the effect of using a simplified propeller model becomes clear. The asymmetry in the flow is not accurately captured due to the non-uniform inflow into the propeller plane not being included in the body force model. An important observation may be made by analysing the effect of the ESD boundary layer on the predicted and measured axial velocity contours in Figure 11. This is not visible in the OpenFOAM case, however. The reason is that the StarCCM+ simulation used an all y+ boundary layer model, whereas the open-source counterpart fully resolved the boundary layer. Due to a very low Reynolds number of the duct (25000 based on chord and free-stream velocity) the more explicit approach does not yield satisfactory results. On the other hand, the wall-function approach leads to duct wake being seen around top-dead centre, which is not seen in the experiment.

8. DISCUSSIONS

Flow analysis of the flow around the JBC has indicated that it is affected by several phenomena challenging from the numerical point of view. Among the most prominent are a strong hook-shaped vortex around the aft bilge, an area of separated flow below the hub just upstream of the propeller plane. The existence of both will have a substantial effect on the propeller efficiency and its optimum design, and hence understanding these flow features is of key importance. Although further analysis of the present data set is needed to show this for the considered hull, Wackers et al., (2015) have indicated on the example of the KVLCC2, subject to a similar flow regime that turbulence in the aforementioned regions may be highly anisotropic due to substantial twist in the boundary layer. This poses an important question of whether application of a RANS turbulence model based on the Boussinesq hypothesis to complex ship flows may be justified with more advanced methods, such as Reynolds Stress Models or Detached Eddy Simulation, becoming more available with increasing computational power.

Another important issue visible in the computational results is the difference of scales between the hull and the energy saving device. The small size of the latter requires a significantly higher mesh resolution than would normally be required for a ship self-propulsion simulation, increasing the computational effort substantially. More importantly, it poses restrictions on the numerical method being used, particularly at model scale where very low Reynolds numbers may be expected. This further decreases confidence in predictions made using the standard RANS turbulence models, such as k-ω SST. Given the strong dependence of most energy saving devices on the thickness of the hull boundary layer, local characteristics of turbulence, and the presence of flow separation, one may also be concerned with whether model-scale experiments and fluid dynamic computations may be used to deduce ESD efficiency at full scale.

9. CONCLUSIONS

Results of the numerical computations of the JBC hull form using both open source CFD code OpenFOAM and a commercial code StarCCM+ showed little difference in the predicted forces and flow fields. However, comparison of the flow patterns to measured data showed that improvements could still be made. In particular, using a more appropriate turbulence modelling technique, such as Detached Eddy Simulation, should help in capturing the fine detail of separated flow in the aft part of the hull and using a fully-modelled propeller instead of a simple actuator disk approach may improve the self-propulsion results.

10. ACKNOWLEDGEMNETS

The authors acknowledge the use of the IRIDIS High Performance Computing Facility, and associated support services at the University of Southampton in completion of this work.

REFERENCES

Couser, P., Wellicome , J., and Molland, A., 1998. An improved method for the theoretical prediction of the wave resistance of transom-stern hulls using a slender body approach. International Shipbuilding Progress, 45, 331-349.

Goldstein, S., 1929. On the Vortex Theory of Screw Propellers. Proc. of the Royal Society, 123, 440, (A).

Hough, G.R. and Ordway, D.E., (1965), The generalized actuator disc. Developments in theoretical and applied mechanics, 2, 317-336.

Larsson, L., Stern, F. and Visonneau, M. (2014),"Numerical Ship Hydrodynamics – An assessment of the Gothenburg 2010 Workshop", Springer

OpenCFD and The OpenFOAM Foundation (2014), "OpenFOAM Version 2.3.0".

Menter, F.R., 1994. Two-equation eddy viscosity turbulence models for engineering applications. AIAA journal, 32(8), pp.1598–605.

NMRI., 2015. Tokyo 2015, A Workshop on CFD in Ship

Hydrodynamics. Retrieved from http://www.t2015.nmri.go.jp/ User Guide version STAR-CCM+ 9.04.

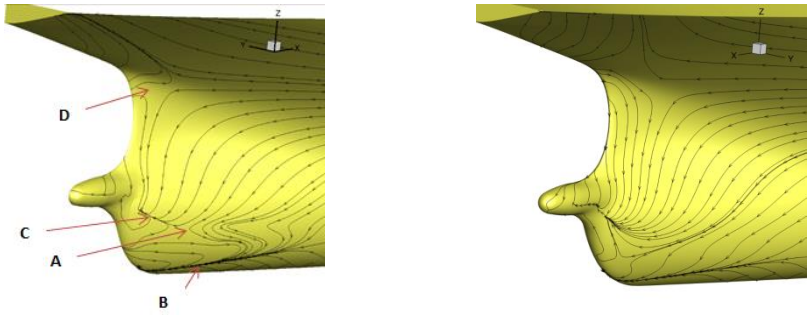

[a] [b]

Fig.4 Limiting streamlines [a] nominal [b] effective without ESD using OpenFOAM.

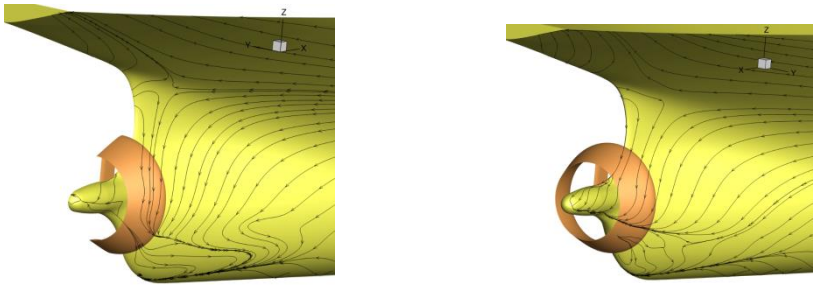

[a] [b]

Fig.5 Limiting streamlines [a] nominal [b] effective with ESD using OpenFOAM. .

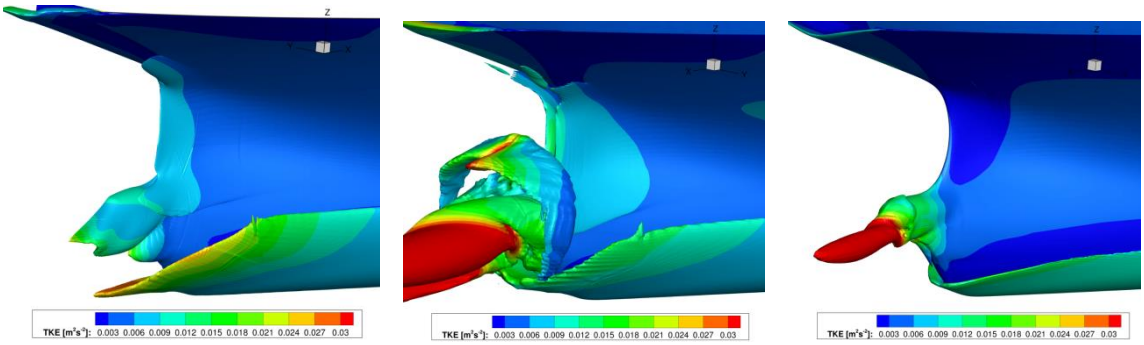

[a] [b] [c]

Fig.6 Vortical structures around the stern [a] nominal, 25s-1[b] effective, 25s-1 [c] effective, 65s-1 without ESD using OpenFOAM. Isocontours are coloured by turbulent kinetic energy.

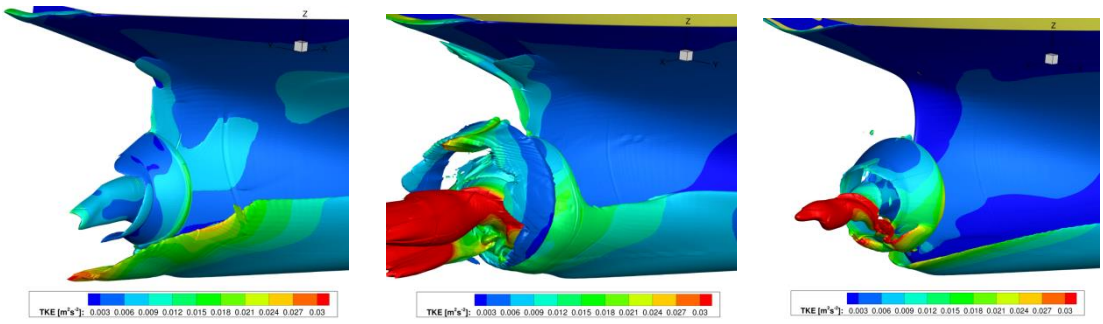

[a] [b] [c]

Fig.7 Vortical structures around the stern [a] nominal 25s-1[b] effective, 25s-1 [c] effective, 65s-1with ESD using OpenFOAM. Isocontours are coloured by turbulent kinetic energy.

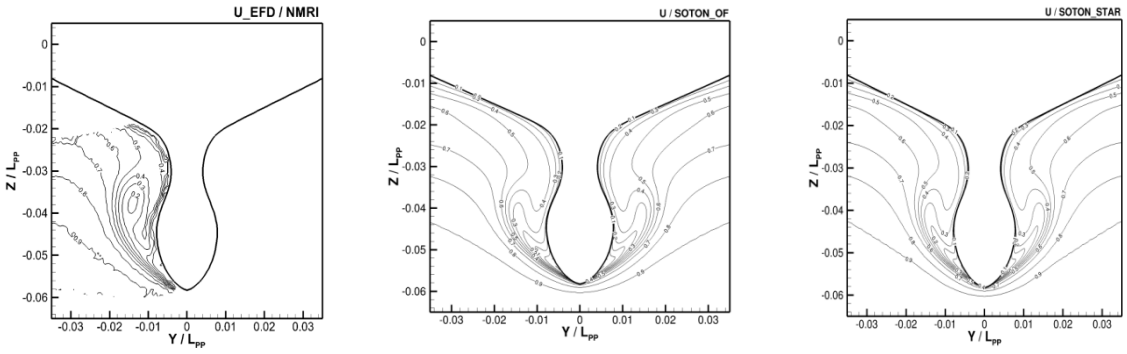

Fig.8 Results of mean axial velocity at x/Lpp = 0.9625 with ESD in the towed condition. Experiment (left), OpenFOAM (middle), StarCCM+ (right).

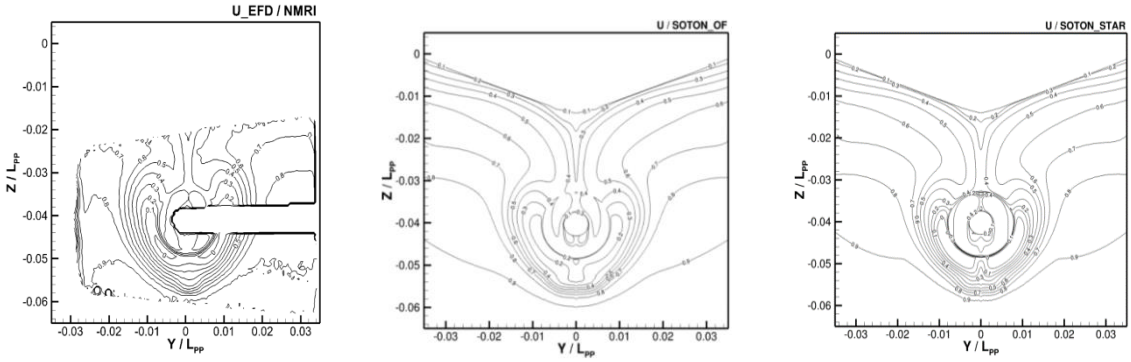

Fig.9 Results of m ean axial velocity at x/Lpp = 0.9843with ESD in the towed condition. Experiment (left), OpenFOAM (middle), StarCCM+ (right).

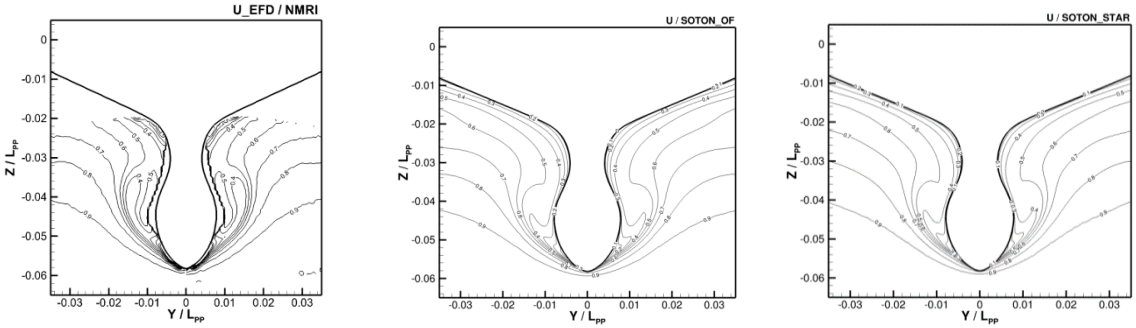

Fig.10 Results of mean axial velocity at x/Lpp = 0.9625 without ESD in the self-propelled condition. Experiment (left), OpenFOAM (middle), StarCCM+ (right).

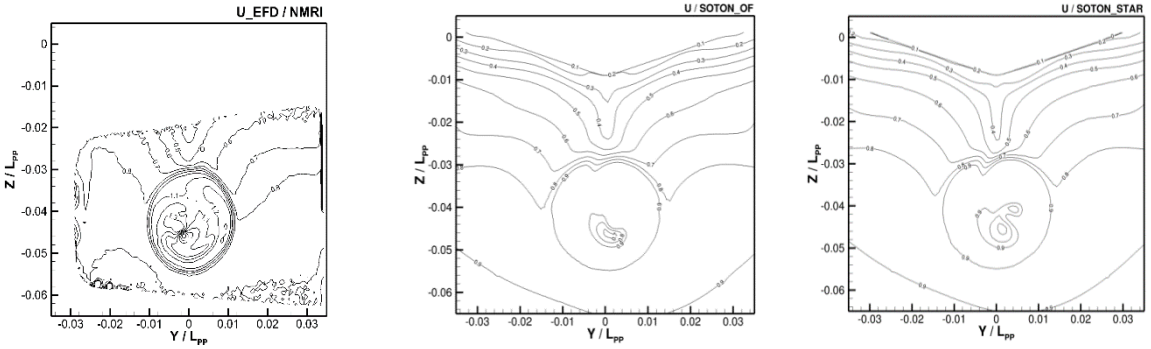

Fig.11 Mean axial velocity at x/Lpp = 0.9843 without ESD in the self-propelled condition. Experiment (left), OpenFOAM (middle), StarCCM+ (right).